Biochemical and Biophysical Research Communications 391 (2010) 340–345

Contents lists available at ScienceDirect

Biochemical and Biophysical Research Communications

journal homepage: www.elsevier.com/locate/ybbrc

A new activity of anti-HIV and anti-tumor protein GAP31: DNA adenosine glycosidase – Structural and modeling insight into its functions ☆

Hui-Guang Li [a], Philip L. Huang [b,1], Dawei Zhang [a], Yongtao Sun [a], Hao-Chia Chen [c], John Zhang [d], Paul L. Huang [e,1], Xiang-Peng Kong [a,*], Sylvia Lee-Huang [a,*,1]

[a] Department of Biochemistry, New York University School of Medicine, New York, NY 10016, USA
[b] American Biosciences, Boston, MA 02114, USA
[c] Endocrinology and Reproduction Research Branch, National Institute of Child Health and Human Development, NIH, Bethesda, MD 20892, USA
[d] Department of Chemistry, New York University, New York, NY 10003, USA
[e] Department of Medicine, Harvard Medical School and Massachusetts General Hospital, Boston, MA 02114, USA

ARTICLE INFO

Article history:
Received 2 November 2009
Available online 12 November 2009

Keywords:
AIDS
HIV-1
Antiviral
Anti-tumor
Adenosine glycosidase
Plant protein

ABSTRACT

We report here the high-resolution atomic structures of GAP31 crystallized in the presence of HIV-LTR DNA oligonucleotides systematically designed to examine the adenosine glycosidase activity of this anti-HIV and anti-tumor plant protein. Structural analysis and molecular modeling lead to several novel findings. First, adenine is bound at the active site in the crystal structures of GAP31 to HIV-LTR duplex DNA with 5′ overhanging adenosine ends, such as the 3′-processed HIV-LTR DNA but not to DNA duplex with blunt ends. Second, the active site pocket of GAP31 is ideally suited to accommodate the 5′ overhanging adenosine of the 3′-processed HIV-LTR DNA and the active site residues are positioned to perform the adenosine glycosidase activity. Third, GAP31 also removes the 5′-end adenine from single-stranded HIV-LTR DNA oligonucleotide as well as any exposed adenosine, including that of single nucleotide dAMP but not from AMP. Fourth, GAP31 does not de-purinate guanosine from di-nucleotide GT. These results suggest that GAP31 has DNA adenosine glycosidase activity against accessible adenosine. This activity is distinct from the generally known RNA *N*-glycosidase activity toward the 28S rRNA. It may be an alternative function that contributes to the antiviral and anti-tumor activities of GAP31. These results provide molecular insights consistent with the anti-HIV mechanisms of GAP31 in its inhibition on the integration of viral DNA into the host genome by HIV-integrase as well as irreversible topological relaxation of the supercoiled viral DNA.

Introduction

GAP31 (Gelonium Anti-HIV Protein, 31 kDa) is isolated from the seeds of *Gelonium multiflorum* [1]. It inhibits not only *de novo* HIV-1 infection and cell-to-cell transmission of the virus, but also viral replication in already infected cells [1–3], affecting multiple targets of HIV-1 including viral entry, viral genome integration and topology of viral DNA [1–3]. GAP31 is not toxic to uninfected target cells, human spermatocytes or intact animals [1,4,5]. In addition to HIV-1, it is effective against Herpes Simplex Viruses (HSV) [6] and Human Herpes Virus 8 (HHV8) [7]. GAP31 was tested against a panel of 58 human tumor cell lines representing nine cancer types by National Cancer Institute (NCI). Potent anti-tumor activity was observed against melanoma, brain and breast cancer cell lines [8]. *In vivo* studies demonstrated that GAP31 effectively prevented tumor development in SCID mice xenografted with human breast tumor MDA-MB-231 [5]. In addition to tumor and viral targets, GAP31 modulates the expression of host genes related to tumorigensis, signal transduction, apoptosis, proliferation, stress and infection [3,7].

To define the molecular mechanism of GAP31 in HIV-1 integrase inhibition, we carried out systematic crystallographic examinations of the DNA glycosidase activity of GAP31. We first determined the crystal structure of native GAP31 to 1.6 Å resolution. Then, we co-crystallized GAP31 with various DNA substrates based on the structure of HIV-1 LTR. We also used di- and mononucleotides and determined nine co-crystal structures of GAP31, all to about 2.0 Å resolution. High-resolution atomic structural analysis demonstrated that binding of adenine at the GAP31 active

☆ Supported by PHS Grants R01-AT01383, R01-AI31343 to S.L.-H. and J.T. Research Grant to S.L.-H. and X.P.K.

* Corresponding authors. Fax: +1 212 263 8166 (X.-P. Kong), +1 212 263 8166 (S. Lee-Huang).
E-mail addresses: xiangpeng.kong@med.nyu.edu (X.-P. Kong), sylvia.lee-huang@med.nyu.edu (S. Lee-Huang).

[1] Dedication: This paper is dedicated to the memory of Mrs. An Fu Lee, devoted and beloved mother and grandmother.

0006-291X/$ - see front matter © 2009 Elsevier Inc. All rights reserved.
doi:10.1016/j.bbrc.2009.11.060

site correlates highly with the structure of the substrates. GAP31 binds to adenine bases in DNA that are accessible to the enzyme, including those in single-stranded DNA, unpaired duplex ends and single nucleotides. Molecular modeling on the interaction between GAP31 and HIV-LTR DNA offers molecular explanations for the inhibition of GAP31 on HIV-integrase in the integration of viral DNA into host genome.

Experimental methods

Nucleotides and DNA oligonucleotides. dAMP (deoxyadenine 5′-monophosphate) and AMP (adenosine 5′-monophosphate) were purchased from Sigma. Di-deoxynucleotides, GT and AC, and oligodeoxynucleotide substrates were synthesized by Genemed, Inc. Three types of substrates corresponding to the nucleotide sequences of the U5 end of HIV-LTR were prepared: blunt-ended, 5′ overhanging and self-complementary. To generate the first two types, we synthesized a single nucleotide strand of 21 bases representing the U5 region of the HIV-LTR, ss21A (5′-ACTGCTAGAGATTTTCCACAC-3′), its complementary strand ss21B (5′-GTGTGGAAAATCTCTAGCAGT-3′), and a 19 base strand with the 3′-di-nucleotide GT removed from ss21B, refer to as ss19B (5′-GTGTGGAAAATCTCTAGCA-3′). We also designed and synthesized two self-complementary oligonucleotides of 22 and 24 bases, designated hp22 (5′-ACTGCTAGAGTTCCCTCTA GCA-3′) and hp24 (5′-ACTGCTAGAGTTCCCTCTAGCAGT-3′). hp22 and hp24 self-anneal and form secondary structure mimicking HIV-LTR U5.

Preparation and purification of double-stranded DNA oligonucleotides. Double-stranded oligonucleotide substrates ds21A-21B (U5LTR) and ds21A-19B (dsU5-GT) were prepared as described previously [2]. The annealed double-stranded complexes were purified by native polyacrylamide gel electrophoresis using a 15% gel in Tris–boric acid–EDTA buffer. The self-complementary oligonucleotides hp22 and hp24 with a four-base (5′-TTCC-3′) loop as underlined in the sequence above were prepared by annealing at 95 °C for 10 min and cooled slowly.

Crystallization of the GAP31 and complexes. Homogeneous GAP31 protein was isolated and purified from mature seeds of *G. multiflorum* as previously described [1,3,9,10]. Crystals of GAP31 were obtained with hanging drop vapor diffusion method by mixing 1 μl of GAP31 solution (15 mg/ml) with 1 μl of well solution containing 100 mM Tris–HCl, pH 8.5, and 2 M $(NH_4)_2SO_4$. Crystals grew in 2 weeks at 27 °C. Complex crystals of GAP31 were obtained by either soaking the native crystals for 48 h with dAMP, AMP, the di-deoxynucleotides AC or GT (5 mg/ml in the well solution) or co-crystallizing GAP31 with DNA oligonucleotides at a fivefold excess molar ratio. To transport the crystals to synchrotron beamlines for X-ray diffraction data collection, crystals were transferred into the well solution containing in addition 30% glycerol and frozen in liquid propane.

Data collection, structure determination and refinement. The X-ray diffraction data were collected at synchrotron beamline X12B, X26C of National Synchrotron Light Source (NSLS), Brookhaven National Laboratories and beamline 19-ID Argonne National Laboratory Structural Biology Center of Advanced Photo Source (APS). Crystals of the GAP31 and complexes diffracted to better than 2 Å and were in the space group $P2_1$ with lattice constants of $a = 48$ Å, $b = 44$ Å, $c = 137$ Å, $\beta = 98°$ (Table 1). All data sets were integrated and scaled using the HKL package [11]. GAP31 structure was determined by molecular replacement using the program AMoRe [12] with the ricin A-chain structure (PDB code 1BR6) as the starting model. The data collection statistics are shown in Table 1. Refinement of the structures was carried out by CNS package [13], using O for manual adjustment [14]. All the complex crystal structures were refined using native GAP31 as the initial model and the substrates fitted into the electron density of difference Fourier maps. The secondary structural elements of the model were assigned using program DSSP [15] and the superposition of structures were carried out using ICM [16]. Figs. 1 and 2 were rendered using PyMOL (W.L. DeLano, The PyMOL Molecular Graphics System, DeLano Scientific, San Carlos, CA).

Molecular modeling. Molecular docking of HIV-LTR DNA into the active site of GAP31 was carried out using AutoDock 3.0.5 [17]. The relaxation of docking structure obtained was then implemented under Discovery from Insight II (Accelrys, Inc., San Diego, CA, USA) using 500 steps of Steepest Descent followed by Conjugate Gradient until the root mean square (RMS) of the energy gradient reaches a value of 0.01 kcal/mol Å.

Results and discussion

Structure of GAP31

The crystal structure of native GAP31 was determined by the molecular replacement method using ricin A-chain structure as the starting model, and refined to 1.6 Å resolution (Table 1 and Figs. 1, 2). Each asymmetric unit of the crystal unit cell of space group $P2_1$ has two almost identical GAP31 molecules (with rmsd of 0.038 Å upon superimposition of the C_α atoms) related by a non-crystallographic twofold axis (Fig. 1). Each GAP31 molecule contains eight major helices and three beta sheets, one of six strands and two of two strands (Fig. 1). The structure of GAP31 is highly homologous to other type I RIPs and A-chain of type II RIPs, although the amino acid sequences are only about 35% identical. For example, the rmsd of the least square superposition of the C_α trace of GAP31 with ricin A-chain (PDB code 1IFS), abrin A-chain (PDB code 1ABR), PAP (PDB code 1PAF) and trichosanthin (PDB code 1MRJ) is 1.43 Å, 1.41 Å, 1.30 Å and 1.35 Å, respectively, all with more than 90% of GAP31 C_α atoms (equivalences) superimposed. The structure of GAP31 can be artificially

Table 1
Summary of data collection and data statistics.

Crystal	GAP31	AMP	dAMP	AC	GT	ss21A	ss21B	ds21A-21B	s21A-19B	hp24	hp22
Space group	$P2_1$	$P2_1$	$P2_1$	$P2_1$	$P2_1$	$P2_1$	$P2_1$	$P2_1$	$P2_1$	$P2_1$	$P2_1$
Cell parameter											
a(Å)	48.37	47.96	48.04	47.86	48.17	48.15	47.91	48.13	48.07	48.13	48.59
b(Å)	44.40	44.37	44.30	44.21	44.32	44.23	44.20	44.27	44.32	44.30	44.73
c(Å)	137.27	137.01	137.31	137.38	136.85	137.35	137.47	137.05	137.04	137.03	138.70
High-resolution (Å)	1.6	1.9	2.0	1.9	2.0	2.0	1.9	1.9	2.0	2.0	2.0
Reflections											
Total	228,644	154,318	133,481	133,078	138,042	140,147	173,923	175,842	143,159	121,824	121,510
Unique	65,240	46,861	38,469	46,674	37,684	38,588	44,733	43,952	38,892	36,924	37,480
$>2\sigma$	63,424	41,044	37,026	39,942	35,089	37,953	43,262	43,464	38,532	34,520	35,957
R_{merge} (%)	3.6	3.9	3.8	4.1	4.2	3.5	4.6	2.6	4.7	6.9	4.1
Completeness (%)	99.2	97.5	99.1	96.4	98.4	98.6	99.6	97.7	99.4	95.9	96.9

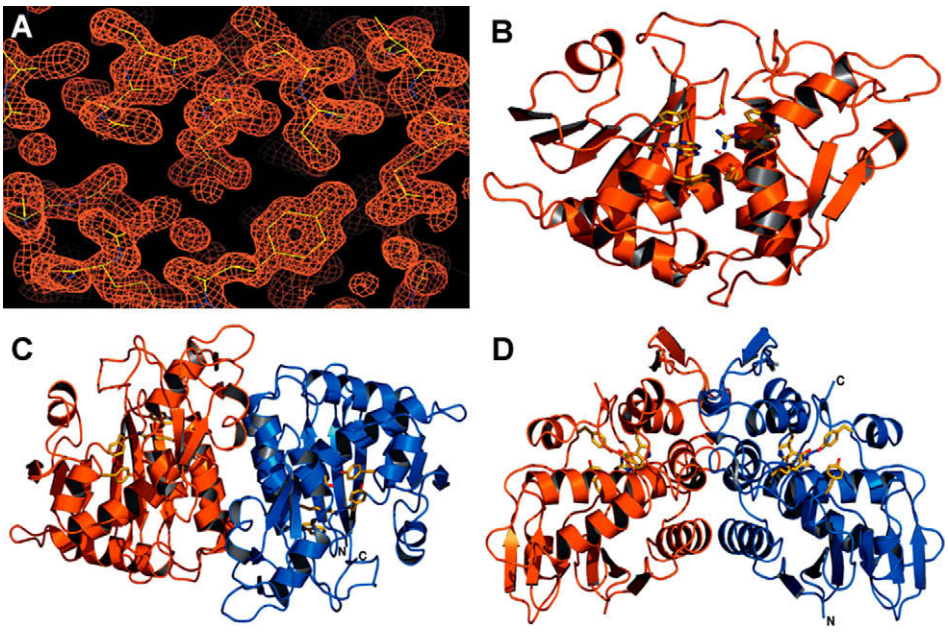

Fig. 1. Electron density map of GAP31 and ribbon representation of native GAP31 structure as a dimer in the crystallographic asymmetric unit. (A) High-resolution (1.6 Å) density map of GAP31. The region around Tyr113 of the refined $2F_o - F_c$ electron density map of the native GAP31 is displayed by program O (contoured at 1.0σ). Tyr113 has a poorly defined electron density in native GAP31 (without bound substrate). (B) The crystallographic GAP31 dimer, a view looking down from the twofold axis. The ribbons of the two molecules are colored orange and blue. The side chains of the active site amino acids are shown. (C) The dimer is rotated by 90° from (B). (D) The N-terminus and C-terminus of the molecule colored blue is indicated.

divided into either three domains, as in the case of ricin A-chain [18], or two domains, as in the case of α-momorcharin [19]. The active pocket is located at the cleft between these subdomains. The C-terminus of GAP31 is located close to the active site, whereas the N-terminus is located on the other side of the molecule (Fig. 2). Residues Cys44 and Cys50 are well positioned to form a disulfide bond. *N*-Glycosylation at residue Asn189 is clearly visible and the first moiety of the sugar is built into the density and refined. The side chain of Asn189 is exposed to the solvent, about 20 Å away from the active site. This is consistent with the fact that glycosylation is not required for the enzymatic function of GAP31 [20].

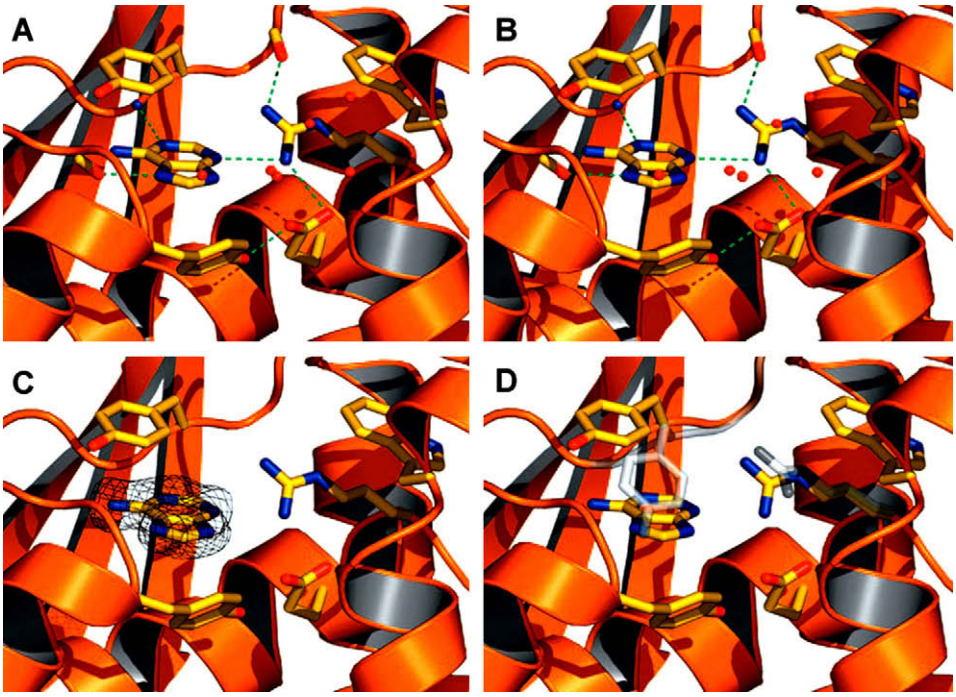

Fig. 2. Structure of GAP31 complexed with adenosine. (A) Ribbon representation of GAP31 with adenosine bound at its active site. Side chains of the key amino acids at the active site are shown as sticks. (B) Stereo view showing the details of the active site. Possible hydrogen bonds are displayed as dashed lines. (C) Electron density of the adenine substrate is contoured at 1.0 Å level. (D) Superposition of the active site of the native (gray) GAP31 and that of the complexed one (colored). Note that the side chain of Tyr74 makes a large movement upon adenine binding.

Relation of adenine binding with the DNA oligonucleotide sequences

The DNA adenine glycosidase activity of GAP31 was investigated by co-crystallization of DNA oligonucleotide substrates with GAP31. All crystal structures were determined and refined to high-resolution (Table 2). These structures are almost identical (rmsd of superposition of C_α atoms is in the range of 0.12–0.17 Å), except the active pocket. Adenine was found in the active site only with GAP31/ss21A, GAP31/ss21B, GAP31/ds21A-19B, GAP31/hp22, GAP31/AC and GAP31/dAMP, but not with other substrates (Table 2). These results are consistent with the known effects of GAP31 in removing the 5′-end adenine from single-stranded DNA oligonucleotides, as in the cases of GAP31/ss21A and GAP31/ss21B. It does not remove adenine from duplex DNA oligonucleotides with blunt ends, as in the cases of GAP31/ds21A-21B and GAP31/hp24. However, it does remove adenine from duplex DNA with 5′ overhanging adenosine ends, as in the cases of GAP31/ds21A-19B and GAP31/hp22. In addition of removing adenine from di-nucleotides 5′-AC-3′, GAP31 also releases adenine from dAMP but not from AMP. Furthermore, GAP31 does not de-purinate guanosine from di-nucleotide GT. These results suggest that GAP31 has DNA adenosine glycosidase activity against accessible adenosine and may even have broader specificity against DNA than against RNA.

Structure of the active site pocket of GAP31

The active site of GAP31 is located in a cleft of the molecule formed largely by residues highly conserved for RIPs (Fig. 2), including Tyr74, Tyr113, Glu166, Arg169 and Trp198, which form a cluster at the bottom of the cleft [21]. They also form a hydrogen-bonding network centered at Glu166 (Fig. 2): its side chain can form a hydrogen bond with Tyr113 as well as Arg169, which in turn forms a hydrogen bond with the carbonyl oxygen of Ser72. The side chain of Arg169 packs parallel against the side chain of Trp198 located across from Tyr74 at the bottom of the cleft. The active site residues stay largely unchanged upon adenine binding, except Tyr74 (Fig. 2). For the native molecule, the side chain of Tyr74 points toward Tyr113 and the hydroxyl oxygen of Tyr74 can form a hydrogen bond with the carbonyl oxygen of Gly111. Upon adenine binding, the side chain of Tyr74 rotates ~35° away from Tyr113 resulting in its hydroxyl oxygen moving about 5 Å (so that it can now form a hydrogen bond with the side chain of Glu89) even though the C_α atom moved only ~0.85 Å. This movement makes it possible to sandwich the adenine molecule between Tyr74 (on top) and Tyr113 and Ile161 (on the bottom). While Tyr113 in the complex structure has a well-defined electron density, it is the only residue in the core region of the molecule that has a poorly defined electron density in the native structure (Fig. 1). The side chain of Tyr74 may have alternative conformations; it may serve as a "door" that can swing open to let in the substrate. The guanidinium group of Arg169, which is thought to be a critical residue of the *N*-glycosidase catalysis [22], moves slightly toward the substrate upon adenine binding so that its side chain is at a hydrogen-bonding distance from N3 of the adenine molecule (Fig. 2). The carbonyl oxygen of Gly111 can now make a hydrogen bond with the N7 atom of the adenine, instead of the hydroxyl oxygen of Tyr74 as in the native structure (Fig. 2). There are also several water molecules bound at the active side for both the native structure and the complexed one, consistent with their roles in hydrolysis [18,23].

Alignment of all the 39 non-fragment protein sequences of RIPs (rRNA *N*-glycosidase, EC 3.2.2.22) currently listed in the Swiss-Prot database shows that the active site residues, Tyr74, Tyr113, Glu166, Arg169, Trp198 (GAP31 residue numbers), are strictly conserved. Structural alignment of the available X-ray structures of RIPs also shows that their structural cores and active sites superimpose well. GAP31 is therefore likely to have the same *N*-glycosidase mechanism as that of ricin and other RIPs [18,22]. It is also possible that the DNA glycosidase mechanism of RIPs is the same as their RNA glycosidase mechanism. Arg169 is proposed to play an important role in the RNA glycosidase mechanism of RIPs, either to protonate N3 of adenine (54), or to act as a strong electrostatic stabilizing group to promote electron withdrawal from C1′ to N9 of adenine. This would delocalize the charge from N9 before and after bond cleavage [18]. Thus, formation of a hydrogen bond between the side chain of Arg169 and the 2′ oxygen of the substrate may reduce the catalytic power of Arg169. This would suggest that RIPs may have a more effective enzymatic reaction against DNA, in which there is no 2′ hydroxyl group, than against RNA.

Molecular modeling of HIV-LTR binding to GAP31

To define the molecular mechanism of GAP31 inhibition on the integration of viral DNA into host DNA by the HIV-1 integrase, the interaction between HIV-LTR DNA and GAP31 protein was subjected to molecular modeling. Docking of 3′-processed HIV-LTR U5 with X-ray crystal structure of GAP31 was carried out by AutoDock 3.0.5, using a fully flexible di-nucleotide d(pApC) with GAP31–adenosine complex as a control. As seen in Fig. 3 A the 5′ protruding dA of the 3′-processed U5 HIV-LTR can be docked into the GAP31 active site pocket without much structural change and is energetically favorable. The fact that GAP31 clamps the newly exposed 5′ overhanging dA and renders it unable to serve as substrate for HIV-integrase explains the inhibition of GAP31 on the integration of the viral DNA into the host DNA. Fig. 3C shows the 3′-processed HIV-LTR U5 DNA fragment docked onto the surface of GAP31. The viral DNA was docked onto a space-filling surface model of GAP31 showing the potential binding to the protruding dA in the active site.

Table 2
Refinement statistics and the active site adenine.

Crystal	GAP31*	AMP	dAMP	AC*	GT	ss21A	ss21B	ds21A-21B	ds21A-19B	hp24	hp22
Resolution (Å)	1.6	1.9	2.0	1.9	2.0	2.0	1.9	1.9	1.9	2.0	2.0
R-factor	0.208	0.206	0.204	0.208	0.205	0.207	0.205	0.206	0.205	0.208	0.206
R-free factor	0.223	0.235	0.236	0.231	0.232	0.232	0.233	0.238	0.236	0.240	0.235
rmsd bond length (Å)	0.049	0.062	0.06	0.05	0.06	0.05	0.05	0.057	0.055	0.05	0.056
rmsd bond (°)	1.209	1.244	1.248	1.222	1.233	1.209	1.231	1.226	1.245	1.225	1.241
Number of ordered	211	186	177	182	177	175	180	179	177	173	170
Water molecules ADE in the pocket	No	No	Yes	Yes	No	Yes	Yes	No	Yes	No	Yes

* The coordinates of the native structure of GAP31 and the complex structure derived from GAP31/AC, as a representation for the complex structures, have been deposited in PDB accession codes 3KTZ and 3KU0, respectively.

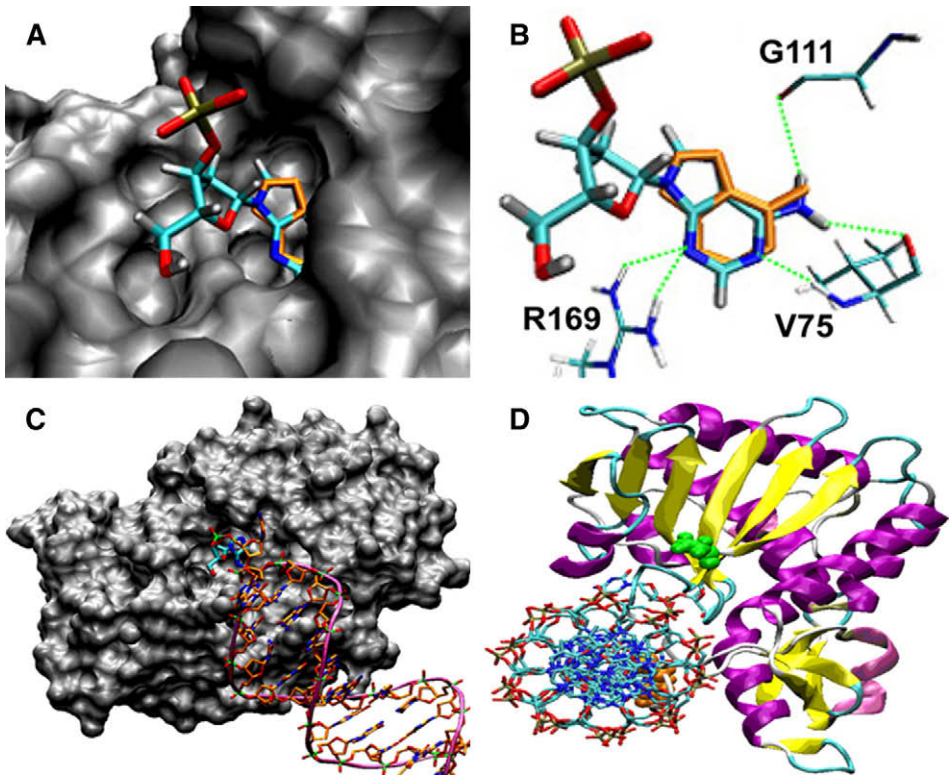

Fig. 3. Molecular modeling of HIV-LTR DNA with GAP31 (A) dAMP deeply seated inside the binding pocket. (B) Hydrogen bonding interaction between dAMP and residues of GAP31 protein. (C) 3′-processed HIV-LTR DNA fragment (21 bp) binding with shown with a gray molecular surface. The HIV-LTR DNA fragment is represented with stick color coded as (a) cyan-carbon, blue-nitrogen and red-oxygen for the unpaired adenine at the 5′-end; (b) orange-carbon, blue-nitrogen, red-oxygen and green-phosphor for the rest of DNA fragment which is highlighted with mauve tube. (D) Docking structure of 3′-processed HIV-LTR DNA fragment (21 bp) binding with GAP31. GAP31 protein is shown in ribbon representation with helices, sheets and turns in purple, yellow and cyan. DNA fragment is colored by element and shown in the stick representation. The two ends of GAP31 are shown with VDW fashion, green for N-terminal and orange for C-terminal, respectively.

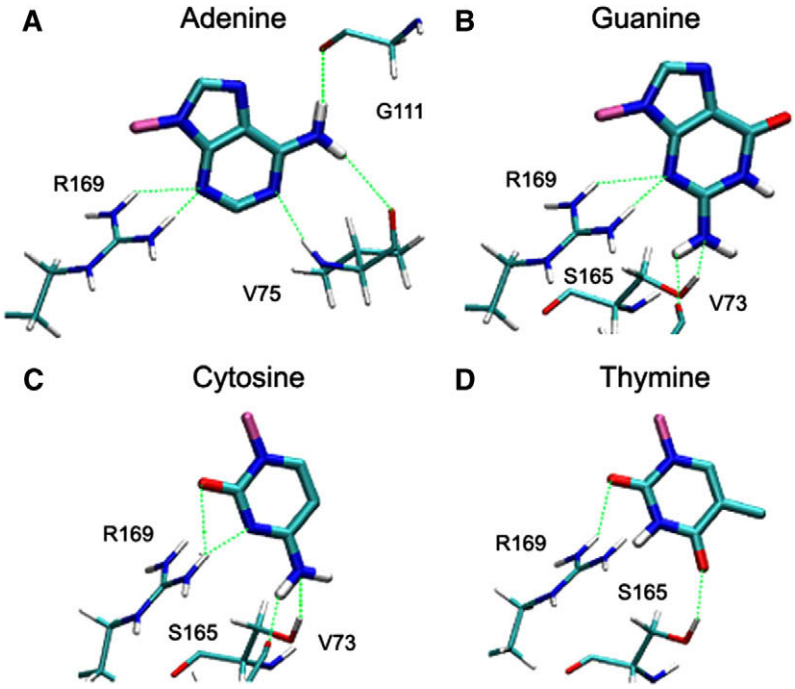

Fig. 4. The docking structures of nucleotide bases within the GAP31 binding pocket. (A–D) Hydrogen bonds between adenine, guanine, cytosine, thymine and residues of GAP31 protein are shown with green dashed lines. The purple dot is connected to the pentose.

Molecular modeling of sequence specificity of GAP31

Our structural results demonstrate that only the 5′ overhanging A is a specific target for GAP31. To model sequence specificity of GAP31, we docked the four bases to the GAP31 binding pocket. Fig. 4 shows the interaction of the adenine with the active center residues. The adenine is deeply seated inside the binding pocket of GAP31, exactly overlapping the adenine in the co-crystal. Arg169, Gly111 and Val75 at the active center are involved in hydrogen bonding with adenine. The guanidinium group of Arg169 is at a hydrogen-bonding distance from N3 of the adenine. The carbonyl oxygens of Gly111 and Val75 are capable of forming hydrogen bonds with the N7 and N1 of the adenine, respectively. There are also several water molecules bound at the active side for both the native structure and the complexes, consistent with roles in hydrolysis [18,22,23].

The predicted binding energies (kcal/mol) for A is −25.5 and for G is −18.5. Cytosine and thymidine are smaller and they do not occupy the active pocket fully. Of the bound bases, adenine makes more extensive interactions with GAP31 than the other three bases (Fig. 4). Mostly, the hydrogen bonds between adenine and the backbone oxygen of Gly111 and Val 75 are lost with guanine.

Conclusion

We have determined the high-resolution structures of native GAP31 and a series of complex structures derived from co-crystallization of GAP31 with systematically designed HIV-LTR DNA oligonucleotide substrates. This is the first report on the co-crystallization and high-resolution atomic structure analyses of GAP31 with DNA substrates. Our results show that the binding of substrate to the active site of GAP31 is sequence and topology specific. GAP31 specifically removes adenine from 5′ overhangs of double-stranded DNA, but not from blunt end double-stranded DNA. In addition, GAP31 acts on exposed 5′ adenosine from single-stranded DNA, oligodeoxynucleotides, di-deoxynucleotides and dAMP, but not from RNA, ribonucleotides and AMP. GAP31 recognizes exposed adenosine specifically but not guanosine, cytosine and thymidine. These results suggest that GAP31 has DNA adenosine glycosidase activity against accessible adenosine and has broader specificity against DNA than RNA. In conclusion, the new high-resolution crystal structure of GAP31 and modeling studies suggest a model where GAP31 caps the 5′ protruding end of HIV-LTR DNA and removes the 5′ adenine, thus preventing integration of viral DNA into the host genome. These results offer valuable insight in rational design of HIV-integrase inhibitors.

Acknowledgments

We thank staff members at X-ray beamlines X12B and X26C of NSLS and 19D of APS for assistance with data collections. This work was supported in part by a JT Research Grant to S.L.-H. and X.P.K. S.L.-H. also acknowledges the support of research Grant R01-AT01383 from the National Center for Complementary and Alternative Medicine (NCCAM) and Grant R01-AI31343 from the National Institute of Allergy and Infectious Diseases (NIAID), NIH.

References

[1] S. Lee-Huang, H.F. Kung, P.L. Huang, B.Q. Li, P. Huang, H.I. Huang, H.C. Chen, FEBS Lett. 291 (1991) 139–144.
[2] S. Lee-Huang, P.L. Huang, A.S. Bourinbaiar, H.C. Chen, H.F. Kung, Proc. Natl. Acad. Sci. USA 92 (1995) 8818–8822.
[3] S. Lee-Huang, P.L. Huang, X. Kong, M. Schapira, P.L. Huang, Res. Dev. Biophys. Biochem. 3 (2003) 235–257.
[4] C.A. Schreiber, L. Wan, Y. Sun, L. Lu, L.C. Krey, S. Lee-Huang, Fertil. Steril. 72 (1999) 686–690.
[5] S. Lee-Huang, P.L. Huang, Y. Sun, H.C. Chen, H.F. Kung, W.J. Murphy, Anticancer Res. 20 (2000) 653–659.
[6] A.S. Bourinbaiar, S. Lee-Huang, Biochem. Biophys. Res. Commun. 219 (1996) 923–929.
[7] Y. Sun, P.L. Huang, J.J. Li, Y.Q. Huang, L. Zhang, S. Lee-Huang, Biochem. Biophys. Res. Commun. 287 (2001) 983–994.
[8] S.M. Rybak, J.J. Lin, D.L. Newton, H.F. Kung, A. Monks, H.C. Chen, P.L. Huang, S. Lee-Huang, Int. J. Oncol. 5 (1994) 1171–1176.
[9] S. Lee-Huang, H.F. Kung, P.L. Huang, A.S. Bourinbaiar, J.L. Morell, J.H. Brown, W.P. Tsai, A.Y. Chen, H.I. Huang, et al., Proc. Natl. Acad. Sci. USA 91 (1994) 12208–12221.
[10] S. Lee-Huang, H.F. Kung, H.C. Chen, P.L. Huang, S.M. Rybak, A.S. Bourinbaiar, F. Musayev, Y.C. Liaw, J. Mol. Biol. 240 (1994) 92–94.
[11] Z. Otwinowski, W. Minor, Methods in Enzymology, vol. 276, Academic Press, 1997, pp. 307–326.
[12] J. Navaza, Acta Crystallogr. D Biol. Crystallogr. 57 (2001) 1367–1372.
[13] A.T. Brunger, P.D. Adams, G.M. Clore, W.L. DeLano, P. Gros, R.W. Grosse-Kunstleve, J.S. Jiang, J. Kuszewski, M. Nilges, N.S. Pannu, R.J. Read, L.M. Rice, T. Simonson, G.L. Warren, Acta Crystallogr. D Biol. Crystallogr. 54 (Pt. 5) (1998) 905–921.
[14] T.A. Jones, J.Y. Zou, S.W. Cowan, M. Kjeldgaard, Acta Crystallogr. A 47 (Pt. 2) (1991) 110–119.
[15] W. Kabsch, C. Sander, Biopolymers 22 (1983) 2577–2637.
[16] R. Abagyan, P. Argos, J. Mol. Biol. 225 (1992) 519–532.
[17] G.M. Morris, D.S. Goodsell, R.S. Halliday, R. Huey, W.E. Hart, R.K. Belew, A.J. Olson, Comput. Chem. 19 (1998) 1639.
[18] W. Montfort, J.E. Villafranca, A.F. Monzingo, S.R. Ernst, B. Katzin, E. Rutenber, N.H. Xuong, R. Hamlin, J.D. Robertus, J. Biol. Chem. 262 (1987) 5398–5403.
[19] J. Ren, Y. Wang, Y. Dong, D.I. Stuart, Structure 2 (1994) 7–16.
[20] P.L. Huang, Y.T. Sun, H.C. Chen, P.L. Huang, S. Lee-Huang, Biochem. Biophys. Res. Commun. 262 (1999) 615–623.
[21] J.A. Chaddock, L.M. Roberts, Protein Eng. 6 (1993) 425–431.
[22] H.G. Li, S.Z. Xu, S. Wu, L. Yan, J.H. Li, R.N. Wong, Q.L. Shi, Y.C. Dong, Protein Eng. 12 (1999) 999–1004.
[23] Q. Guo, W. Zhou, H.M. Too, J. Li, Y. Liu, M. Bartlam, Y. Dong, K.B. Wong, P.C. Shaw, Z. Rao, Protein Eng. 16 (2003) 391–396.